PREDICTIONS OF AMOS OBSERVATIONS OF SPACE SHUTTLE ENGINE FIRINGS

M. Braunstein

Spectral Sciences, Inc., 4 Fourth Ave., Burlington, MA 01803

L. Bernstein

Spectral Sciences, Inc., 4 Fourth Ave., Burlington, MA 01803

R. Dressler

AFRL/VSBXT, Hanscom AFB, MA 01731

M. Venner

104 N. Mercury Blvd, AFRL/PRSA-PS, Edwards AFB, CA 93524

AMOS 2005 CONFERENCE PAPER

1. INTRODUCTION

Engine firings of the Space Shuttle primary control system (PRCS) thrusters can give rise to radiation observable from ground-based telescopes such as AMOS. Such observations would yield valuable information on the environment near the spacecraft during engine operation. The radiation and the mechanisms that produce it are also important to characterize because such radiation can be a significant background noise source for telescopes mounted on spacecraft in low-Earth-orbit or LEO in general [1]. Furthermore, observations of radiation associated with engine firings can give valuable information on fundamental chemical reactions that can be studied over the very large length scales, high energies, and rarefied conditions that are achievable in space but are especially difficult to reproduce in ground-based laboratories.

Radiation associated with Space Shuttle engine firings extending from the ultraviolet region through the infrared has been observed from ground-based, satellite, and on-board sensors [2-9]. The mechanisms that give rise to this radiation are quite diverse. They include combustion products of the space-shuttle engine reacting (either through collisional excitation or chemical reaction) with atomic oxygen in the atmosphere to produce excited state species that then radiate, absorption of sunlight by combustion products that become excited and then radiate, reflection of sunlight from un-combusted engine fuel droplets, and several others. The observed signals appear to be a sensitive function of altitude and atmospheric conditions, spacecraft relative velocity with the atmosphere, and spectral wavelength region. The spatial scale of these signals can extend over several kilometers, reflecting the collision mean-free-path associated with engine exhaust constituents colliding with the atoms and molecules in the rarefied LEO atmosphere.

In this work, we focus on radiation observable in the 2– 5μm (short-wave infrared) region. In this region there are two basic mechanisms known to give rise to observable signals. They are chemical reaction of H_2O from the Shuttle exhaust and atmospheric atomic oxygen to produce excited OH which then radiates,

$$O(^3P) + H_2O(X,^1A_1) \rightarrow OH(X,^2\Pi) + OH(X,^2\Pi)\ ,\ \Delta H = +16.9\ \text{kcal mol}^{-1}, \quad (1)$$

and collisions of H_2O from Shuttle exhaust with atmospheric atomic oxygen to produce internally excited H_2O (collisional excitation) which then radiates,

$$O(^3P) + H_2O(X,^1A_1, (\nu_1\nu_2\nu_3,JK)) \rightarrow O(^3P) + H_2O(X,^1A_1(\nu_1'\nu_2'\nu_3',J'K')). \quad (2)$$

Bernstein *et al.* [6] have shown through analysis of space experiments and laboratory data that the observed radiation from $O(^3P) + H_2O(X,^1A_1)$ collisions may be consistent with either (1) or (2) depending on the collision velocity. Other studies have attributed all such radiation to Reaction (2). It is particularly difficult to distinguish

Report Documentation Page

Form Approved
OMB No. 0704-0188

1. REPORT DATE	2. REPORT TYPE	3. DATES COVERED
22 AUG 2005		**-**

4. TITLE AND SUBTITLE	5a. CONTRACT NUMBER
Predictions of AMOS Observations of Space Shuttle Engine Firings	5b. GRANT NUMBER
	5c. PROGRAM ELEMENT NUMBER

6. AUTHOR(S)	5d. PROJECT NUMBER
Matthew Braunstein; Larry Bernstein; Rainer Dressler; Marty Venner	**5503**
	5e. TASK NUMBER **000P**
	5f. WORK UNIT NUMBER

7. PERFORMING ORGANIZATION NAME(S) AND ADDRESS(ES)	8. PERFORMING ORGANIZATION REPORT NUMBER
Air Force Research Laboratory (AFMC),AFRL/PRSA,10 E. Saturn Blvd.,Edwards AFB,CA,93524-7680	

9. SPONSORING/MONITORING AGENCY NAME(S) AND ADDRESS(ES)	10. SPONSOR/MONITOR'S ACRONYM(S)
	11. SPONSOR/MONITOR'S REPORT NUMBER(S)

12. DISTRIBUTION/AVAILABILITY STATEMENT

Approved for public release; distribution unlimited

13. SUPPLEMENTARY NOTES

14. ABSTRACT

Engine firings of the Space Shuttle primary control system (PRCS) thrusters can give rise to radiation observable from ground-based telescopes such as AMOS. Such observations would yield valuable information on the environment near the spacecraft during engine operation. The radiation and the mechanisms that produce it are also important to characterize because such radiation can be a significant background noise source for telescopes mounted on spacecraft in low-Earth-orbit or LEO in general [1]. Furthermore, observations of radiation associated with engine firings can give valuable information on fundamental chemical reactions that can be studied over the very large length scales, high energies, and rarefied conditions that are achievable in space but are especially difficult to reproduce in ground-based laboratories.

15. SUBJECT TERMS

16. SECURITY CLASSIFICATION OF:			17. LIMITATION OF ABSTRACT	18. NUMBER OF PAGES	19a. NAME OF RESPONSIBLE PERSON
a. REPORT	b. ABSTRACT	c. THIS PAGE			
unclassified	**unclassified**	**unclassified**		**14**	

between (1) and (2) in the 2-5 μm spectral region because OH($X,^2\Pi$) and $H_2O(X,^1A_1)$ have highly overlapping spectral distributions there.

The present work leverages recently published work [10] on the detailed chemistry of O + H_2O to provide signal estimates of PRCS engine firings that could be observed from AMOS. We take into account significant atmospheric absorption effects and show predicted source and apparent spectra and an upper bound on the total observed signal. These calculations are then used to establish sensitivity requirements and assess measurement feasibility with available instrumentation. It is expected that the results will be of great value in preparing for future AMOS observations of Space Shuttle firings. In section 2, we discuss observation scenarios. In section 3, we review detailed data on the chemical mechanisms that give rise to the radiation in order to develop an estimate of the total source signal that is discussed in section 4. In section 5, we discuss atmospheric effects and their impact on the detailed observable spectra and give an estimate of the total apparent signal. In section 6, we discuss instrumentation and signal to noise considerations. In section 7, we give conclusions and discuss possible future work.

2. OBSERVATION SCENARIO

The observation scenario is shown in Fig. 1. Although the exact conditions will depend on the time and details of the particular mission, bracketing general conditions based on previous similar events will be examined. The results from such an analysis can easily be extended to include a particular observation scenario. Many of these observation parameters are derived from an analysis associated with the STS-63 mission where on-board telescopes were used to examine UV radiation associated with Shuttle exhaust [9]. At an operational altitude of ~390 km, the atmosphere is dominated by oxygen atoms whose density is ~5 e13 m^{-3} and whose temperature varies between 700-1000 K. Assuming co-rotation of the thermosphere, the spacecraft velocity with respect to the atmosphere ranges between 7.37 and 7.38×10^3 m s^{-1} for an West-East orbit, depending on the orbiter latitude. We focus on engine firings from the PRCS engines, which use N_2O_4 oxidizer and monomethyl-hydrazine (MMH, chemical formula $(CH_3)HN\text{-}NH_2$) fuel and have an 870 lbf thrust. The gaseous combustion products emanating from the nozzle exit include H_2O, CO, H_2, and N_2, with H_2O at about 1/3 the total mole fraction. The total flux of exhaust gaseous species is ~4.26e25 sec^{-1}. An axial exhaust velocity of 3.5×10^3 m s^{-1} is assumed, which originates from the exit velocity of 3×10^3 m s^{-1} plus an additional 0.5×10^3 m s^{-1} attained in the vacuum expansion. The relative speed between the oxygen atoms in the atmosphere and the exhausting H_2O, which determines the available energy of the collision, is key in determining the level of signal observed. The relative speed is a vector sum of the atmospheric O-atom and H_2O exhaust velocities. It can vary greatly depending on whether the PRCS engines are firing along the wind direction (0 degree or “wake” firing), perpendicular to the wind direction (90 degree or “perpendicular” firing) or against the atmospheric wind direction (180 degree or “ram” firing). For the conditions given above, the relative O-atom/H_2O collision speed is 3.9 km s^{-1}, 8.2 km s^{-1} and 10.9 km s^{-1} for wake, perpendicular, and ram firings, respectively. We also note that the atmospheric temperature implies a spread of O-atom speeds of about 1 km s^{-1}, so that the relative collision speeds will have a ~1.0 km s^{-1} spread around the center values given above. We also note that attenuation effects due to absorption of radiation by CO_2 and H_2O in the atmosphere will be appreciable, and these effects must be taken into account in such an observation scenario.

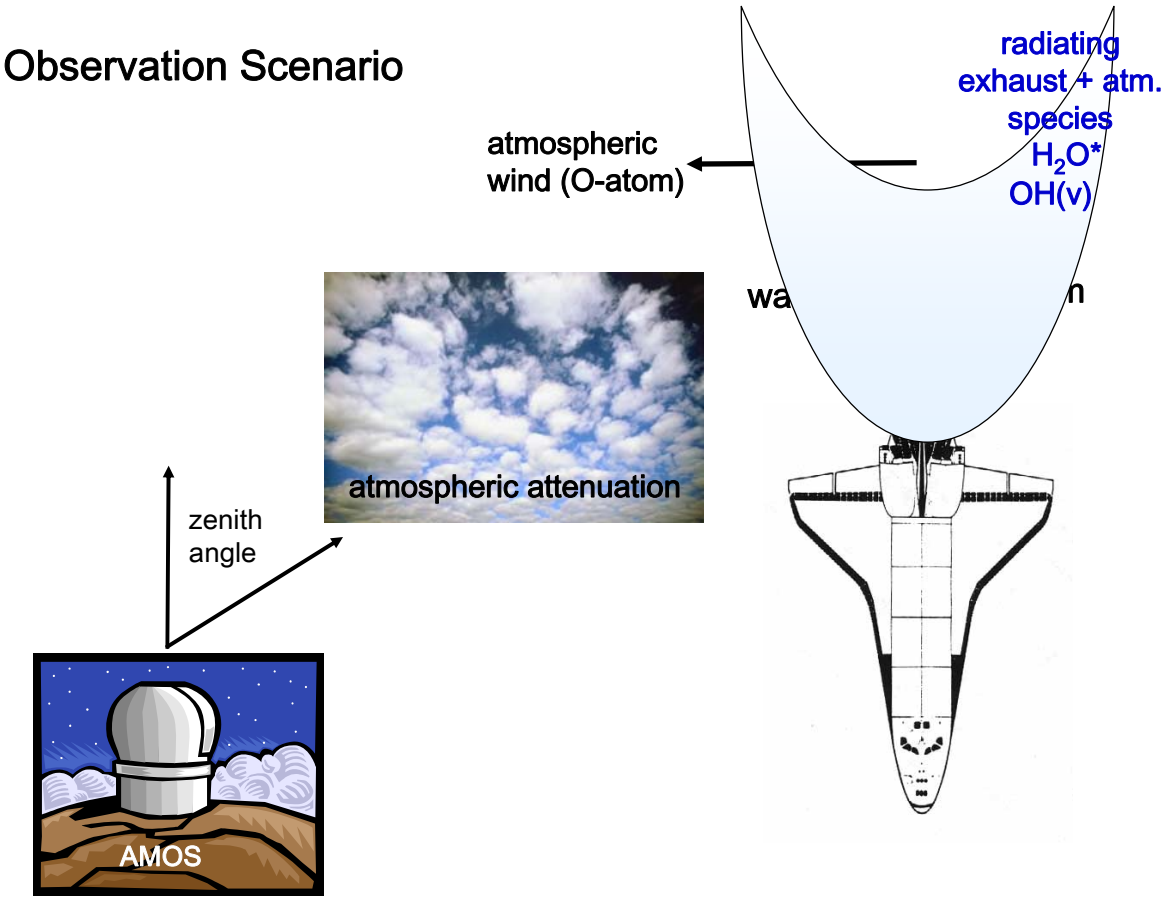

Fig.1. Shuttle engine firing observation scenario. Engine exhaust, consisting mostly of H_2O, interacts with O-atom in the atmosphere to produce internally excited species, OH(v) and H_2O^*. The radiative decay of these excited species is attenuated by the atmosphere and observed from AMOS in the 2-5 μm region.

3. CHEMICAL MECHANISMS

To illustrate the chemical mechanisms involved which produce the observable radiation, we show in Fig. 2 an energy level diagram for O + H_2O collisions with reagents on the left and products on the right against a velocity and energy scale. Creation of product OH(v) and H_2O^* requires significant translational energy. The reagent H_2O has negligible internal energy after expanding into the rarefied atmosphere and the OH(v) and H_2O^* are higher in energy than the cold reagents by a large amount. This implies that wake engine firings, which have a relative O-H_2O collision speed of 3.9 km s^{-1}, will have extremely small signals, as this energy is not enough to produce OH(v>0) and is just above threshold for H_2O^*. Radiation in the 2-5 μm band of interest will occur for creation of populations of OH(v>0) (vibrational excitation beyond the ground state) and for creation of vibrationally excited H_2O, which we denote here as H_2O^*. H_2O has three vibrational modes (ν_1,ν_2,ν_3). Excitation into ν_1 and ν_3 (~10.5 kcal mol^{-1} energy) will fall into the band of interest, while excitation into ν_2, which has a lower energy, will be centered near 6.3 μm (4.5 kcal mol^{-1}).

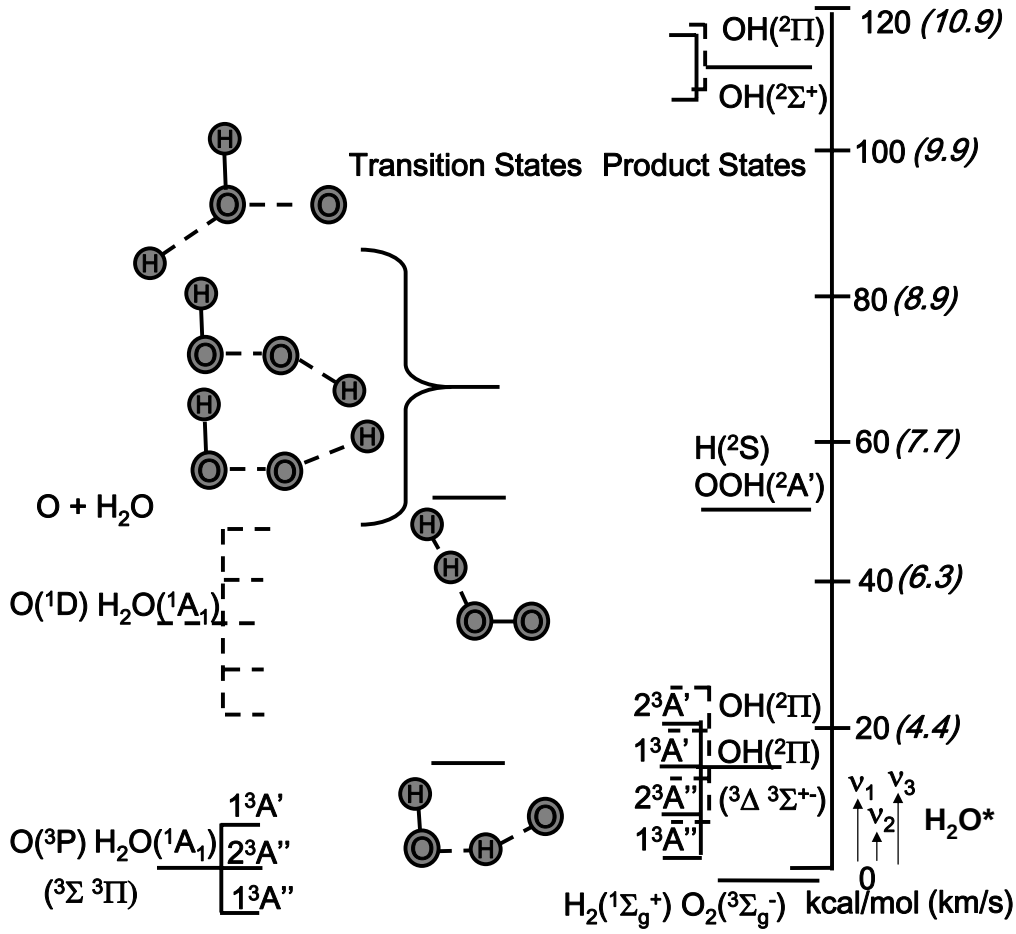

Fig. 2. Energy level diagram of low-lying triplets (solid lines) and singlets (dashed lines) showing reagents, transition states, and products for O + H_2O collisions [10]. The energy and corresponding relative collision velocities are shown in parentheses with respect to the O(^{3}P) + H_2O(X,$^1A_1$) asymptote at zero energy. The energies of the fundamental vibrational modes of H_2O are also shown.

To estimate the observed signal, we adopt a simple model for the total radiation output under steady state (long engine firings) and single-collision (very high altitude) conditions. The spatial region of the radiation will extend several kilometers, and it will be very non-uniform. We do not address the spatial variation of the signal here, and we assume we are capturing all the available radiation. As outlined in [6] and [10], space-based measurements are characterized by a steady-state out-gassing or exhausting source of H_2O with a known or assumed rate, N_{H_2O} (number of H_2O per second), interacting with atomic oxygen in the atmosphere. The signal is observed through a somewhat opaque atmosphere integrated over a wavelength band and characterized by a transmittance, $T_{\Delta\lambda}$. The observed steady state intensity, $I_{\Delta\lambda}^{space}$ (photons s^{-1}), can be written,

$$I_{\Delta\lambda}^{space} \approx \left[\frac{\sigma^*}{\sigma_{tot}}\right] N_{H_2O} T_{\Delta\lambda}\,, \tag{3}$$

where σ_{tot} is the total (reactive and non-reactive) collision cross section for O + H_2O and σ* is the photon excitation cross section which includes all contributions due to photon cascades from multi-quantum excited states. Equation 3 assumes all H_2O molecules collide with atmospheric atomic oxygen once and that all radiation from these collisions

(after being attenuated by the atmosphere) is detected. The ratio, $\left[\frac{\sigma^*}{\sigma_{tot}}\right]$, is the efficiency of producing a photon for a single collision of O + H_2O. For detection in the 2-5 μm spectral region, the intensity will be sensitive to single vibrational quantum changes, so we write the efficiency as,

$$\left[\frac{\sigma^*}{\sigma_{tot}}\right] = \frac{1}{\sigma_{tot}} \sum_{species} \sum_{v=1} v\sigma_v^{species}, \quad (4)$$

where v is the vibrational quantum number, $\sigma_v^{species}$ is the cross section to a particular vibrational state of either collisionally excited H_2O or reaction product OH radiating in the detection band. It is important to emphasize that observations will include contributions from both species. The second sum extends over all possible excited vibrational levels of a given species. Space-based measurements usually assume or otherwise employ models to estimate values for $N_{H_2O}, T_{\Delta\lambda}$ and σ_{tot}, and from the observed intensity, $I_{\Delta\lambda}^{space}$, report a photon excitation cross section, σ*. Therefore, uncertainties in the estimated values of $N_{H_2O}, T_{\Delta\lambda}$ and σ_{tot} are reflected in reported σ*.

The key factor in determining signal levels is the efficiency, Eq. (4). To estimate this efficiency we use the recently determined O + $H_2O \rightarrow$ OH(v) + OH(v) cross sections, Eq. 1, obtained in [10]. These were obtained from computational chemistry modeling of the potential energy surfaces of O + H_2O followed by classical trajectory dynamics calculations to determine cross sections. The results of this modeling showed good agreement with available data, although such data is quite sparse. Fig. 3 shows the cross section as a function of collision velocity derived from the cross sections reported in [10]. It rises steeply from an energy threshold near 4 km s^{-1} for the OH(v=0) product. As the energy increases above the thresholds for the higher OH(v) states, the higher OH states begin to contribute. Also shown is the O + H_2O total cross section, σ_{tot}, taken from [6], $\sigma_{tot} = 2.7e-15\sqrt{2./v_r}$, where v_r is the relative collision speed in units of km s^{-1}, and the resulting total cross section is in units of cm^2. These values for the O + H_2O total cross section are very close to those derived in analysis of observations involving the Russian space station Mir [11].

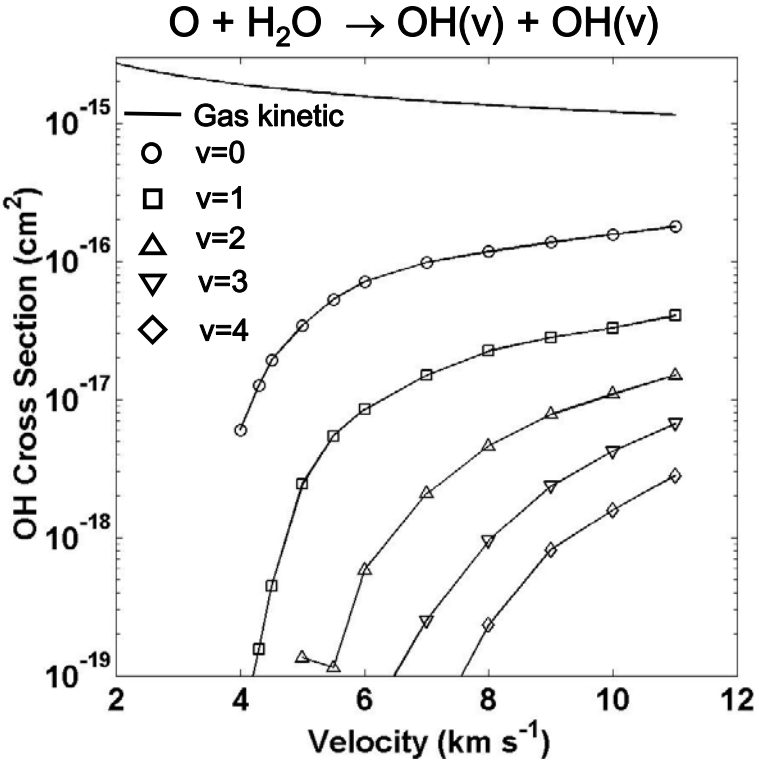

Fig. 3. Cross sections for the reaction, $O + H_2O \rightarrow OH(v) + OH(v)$, as a function of collision velocity, derived from [10]. The H_2O is considered internally cold after undergoing a vacuum expansion. Also shown is the gas kinetic (total) cross section for $O + H_2O$ collisions from [6].

Figure 4 shows the cross sections for excitation of H_2O, $O + H_2O \rightarrow O + H_2O^*$, Eq. 2. These results are new and use the classical trajectory methods outlined in [10] on the same potential surface. The classical trajectory methods used in [10], although convenient for many applications, are not easily amenable to finding vibrationally resolved cross sections for polyatomic molecules, such as H_2O. We therefore use an 'ad-hoc' method of estimating the H_2O^* efficiency from the classical trajectory data. Excitation cross sections are obtained by summing all trajectories where the product H_2O^* has more vibrational energy than the ground state vibrational bin (27.07 kcal mol^{-1}). The curve labeled v'=1 corresponds to H_2O^* whose vibrational energy lies between 27.07 and 31.92 kcal mol^{-1}. The higher bins are incremented in steps of the same width, 4.85 kcal mol^{-1}, the approximate width of the 6.3 μm bin. All bins are labeled as v'=n, where n=1 is the first bin above the vibrational excitation threshold. These excitation cross sections are actually distributed among all the H_2O vibrational excited states (ν_1,ν_2,ν_3). We partition the total H_2O^* (H_2O v>0) cross section into that contributing to 2-5 μm radiation (H_2O 2.7 μm) and that falling outside (dominated by 6.3 μm) in the amounts of 0.15 and 0.85, respectively. This assumption is based on a 'best guess' and represents the weakest part of the signal estimate. We note that near threshold, at least, the relative amounts of 6.3 μm and 2.7 μm H_2O will not be constant as assumed here.

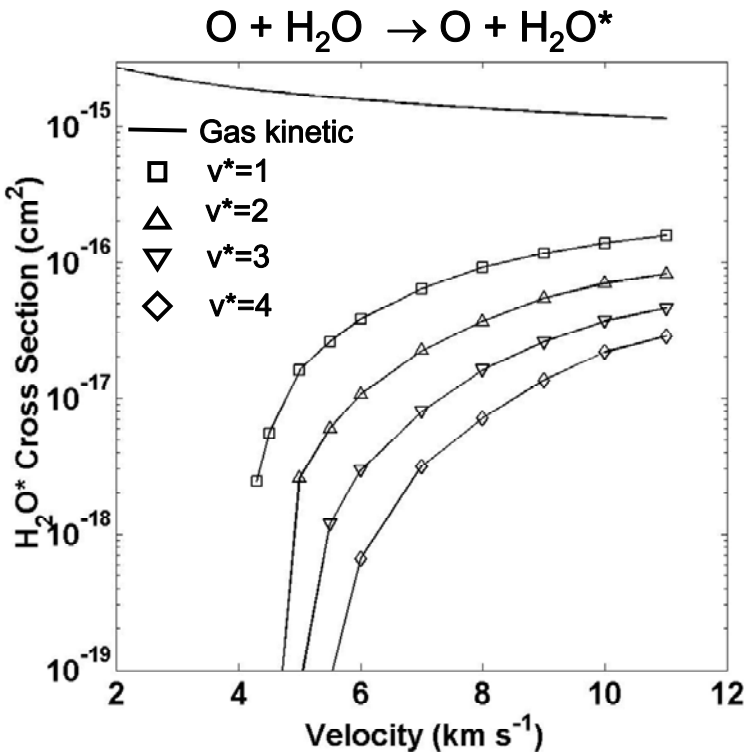

Fig. 4. Cross sections for the reaction, $O + H_2O \rightarrow O + H_2O^*$, as a function of collision velocity, derived using the methods of [10]. The product H_2O^* is split into excited vibrational bins as discussed in the text. Also shown is the gas kinetic (total) cross section for $O + H_2O$ collisions from [6].

4. TOTAL SOURCE (UN-ATTENUATED) SIGNAL

The data shown in Figs. 3 and 4 were translated into total photon efficiencies (Eq. 4), and total signal in units of photon s^{-1} (Eq. 3) at the source (excluding the $T_{\Delta\lambda}$ transmission factor) assuming the PRCS engine parameters previously discussed. These results are shown in Fig. 5 as a function of collision velocity. There are three curves. The curves labeled H_2O 2.7 μm and OH 2.8 μm contribute to the 2-5 μm pass-band. They start from a relatively

small value near threshold and increase rapidly with collision velocity. It is remarkable that the H_2O 2.7 μm contribution and the OH 2.8 μm contribution are nearly identical above threshold. This means that in the total source signal they will contribute about equally. The range of wake, perpendicular, and ram velocities are also shown in the figure. It is clear that wake firings will have a very weak signal. But the source signal will increase greatly as the engine fires into the atmospheric wind (ram direction). This behavior mirrors the threshold effects evident in the vibrational excitation cross sections shown in Figs. 3 and 4.

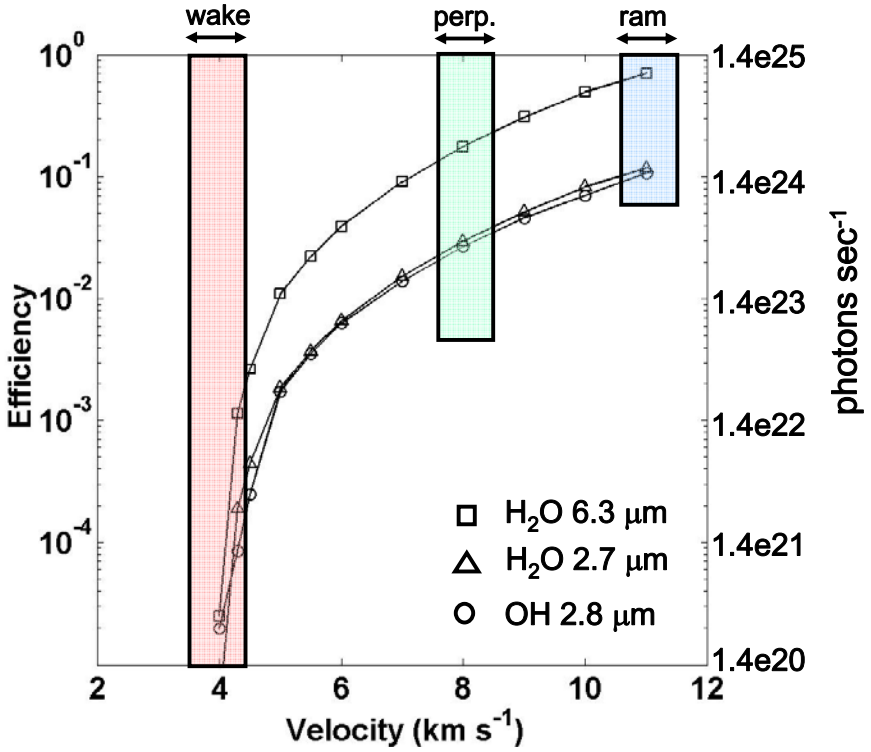

Fig. 5. Photon production efficiency per collision and total source signal in photons s^{-1} as a function of velocity for PRCS engine firings. The H_2O* contribution has been split into H_2O 2.7 μm and H_2O 6.3 μm contributions. The OH(v) contribution is here called 'OH 2.8 μm'. The OH 2.8 μm and H_2O 2.7 μm curves contribute to the 2-5 μm pass-band.

5. ATMOSPHERIC ATTENUATION AND SPECTRAL SIGNALS

Fig. 6 shows spectra computed for OH(v) and H_2O* which have been separately normalized to 1.0, as well as the atmospheric transmittance from a MODTRAN [12] calculation at a 60 degree zenith angle from the AMOS site from 2,000 cm^{-1} to 5,000 cm^{-1} (2-5 μm). The transmittance shows strong absorption by atmospheric H_2O and CO_2. The OH(v) spectra was obtained by running a line-by-line code [13] assuming OH(v,j) populations created at 8 km s^{-1}. The H_2O* spectra was obtained by running a high temperature non-equilibrium code [14] at $T_r = T_v = 1{,}500$ K. This is a best guess at the H_2O* internal temperature. It is interesting that the OH(v) and H_2O* spectral signals are somewhat separated in wavenumber. From this analysis, it is clear that the H_2O* source radiance will be much more attenuated by the atmosphere than the OH(v) radiance. We therefore expect that most of the signal reaching AMOS will be from OH(v).

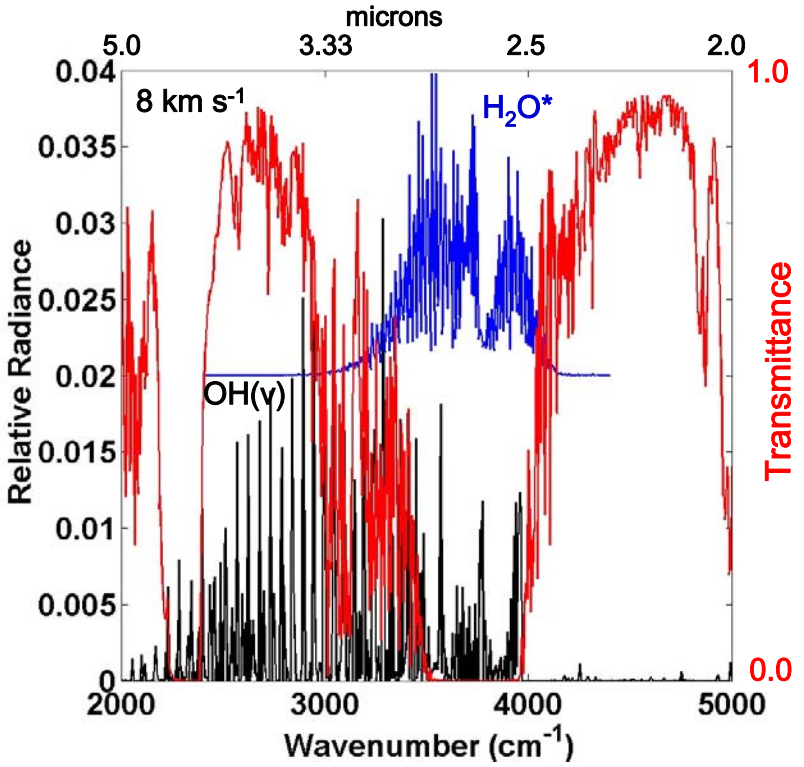

Fig. 6. Normalized spectral radiance from OH(v) (black curve) and H_2O^* (blue curve) at 8 km s^{-1} relative collision velocity. The OH(v) and H_2O^* curves have been separately normalized to 1.0 and the H_2O^* curve displaced for clarity. The atmospheric transmittance for a 60 degree zenith look angle from AMOS is shown in red. Spectral resolution is 5 cm^{-1}.

Fig. 7 shows the total (un-attenuated) source, summing both OH(v) and H_2O^* contributions at 8 km s^{-1}, as well as the total (attenuated) apparent signal. The apparent signal was obtained by multiplying the source signal by the atmospheric transmittance at each spectral bin. The integrated total apparent signal is decreased by a factor of 0.249 by the atmosphere according to this analysis. Because most of the atmospheric attenuation occurs in the same spectral region as the H_2O^* contribution, a very large part of its contribution to the signal disappears in the apparent spectra.

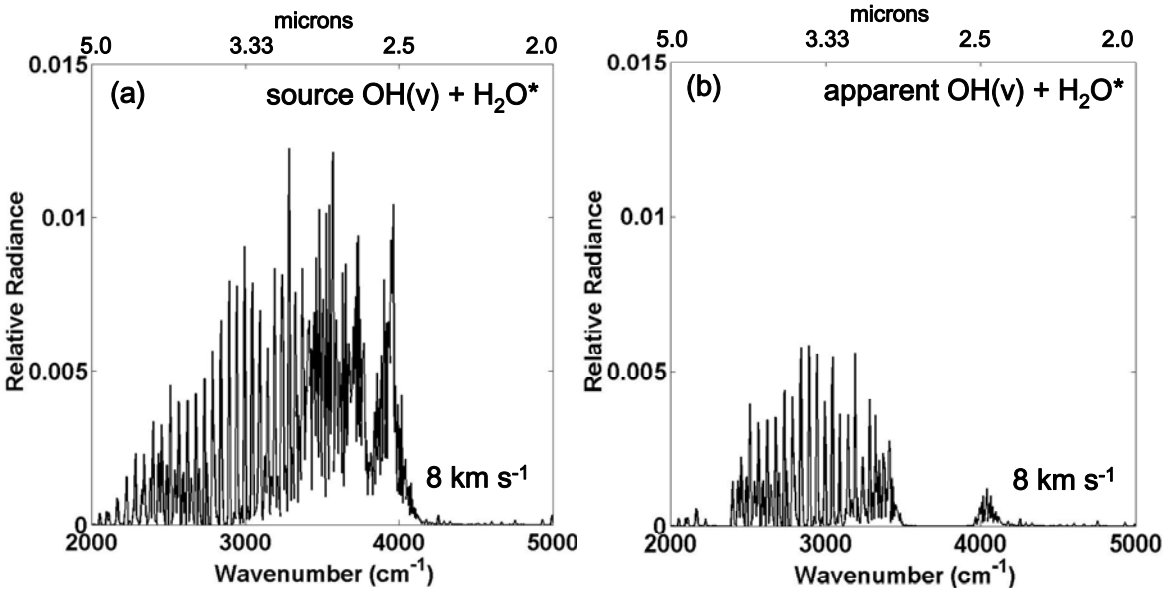

Fig. 7. (a) Source OH(v) + H_2O^* relative spectral radiance at 8 km s^{-1} relative collision velocity. (b) Apparent OH(v) + H_2O^* relative spectral radiance at 8 km s^{-1} relative collision velocity. Here the OH(v) + H_2O^* signal has been attenuated by the atmosphere.

Fig. 8 shows OH(v) and H_2O^* source signal at 11 km s^{-1}. The H_2O^* internal temperature is assumed to be the same as for the 8 km s^{-1} case. The higher collision velocity, however, shifts the OH (v) spectra to higher energy so there is much more overlap with the H_2O^* contribution. This shift also puts the OH(v) contribution much more into the spectral region with large atmospheric attenuation.

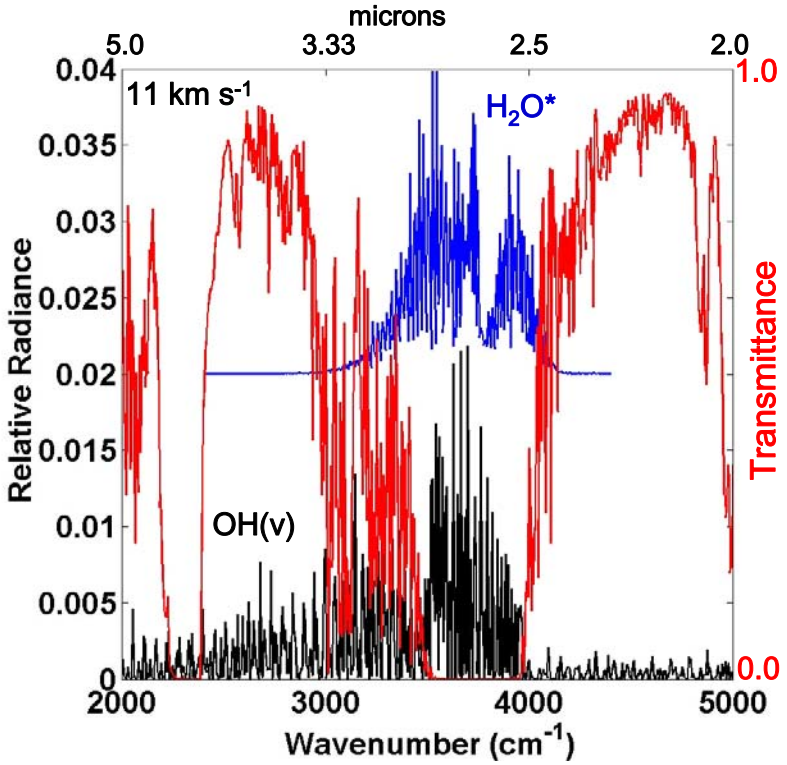

Fig. 8. Normalized spectral radiance from OH(v) (black curve) and H_2O^* (blue curve) at 11 km s^{-1} relative collision velocity. The OH(v) and H_2O^* curves have been separately normalized to 1.0 and the H_2O^* curve displaced for clarity. The atmospheric transmittance for a 60 degree zenith look angle from AMOS is shown in red. Spectral resolution is 5 cm^{-1}.

Fig. 9 shows the total (un-attenuated) source summing both OH(v) and H_2O^* contributions at 11 km s^{-1}, as well as the total (attenuated) apparent signal. The integrated total apparent signal is decreased by a factor of 0.187 by the atmosphere according to this analysis. It is interesting that although we expect more source signal at higher relative velocities (ram firing) we also expect more atmospheric attenuation.

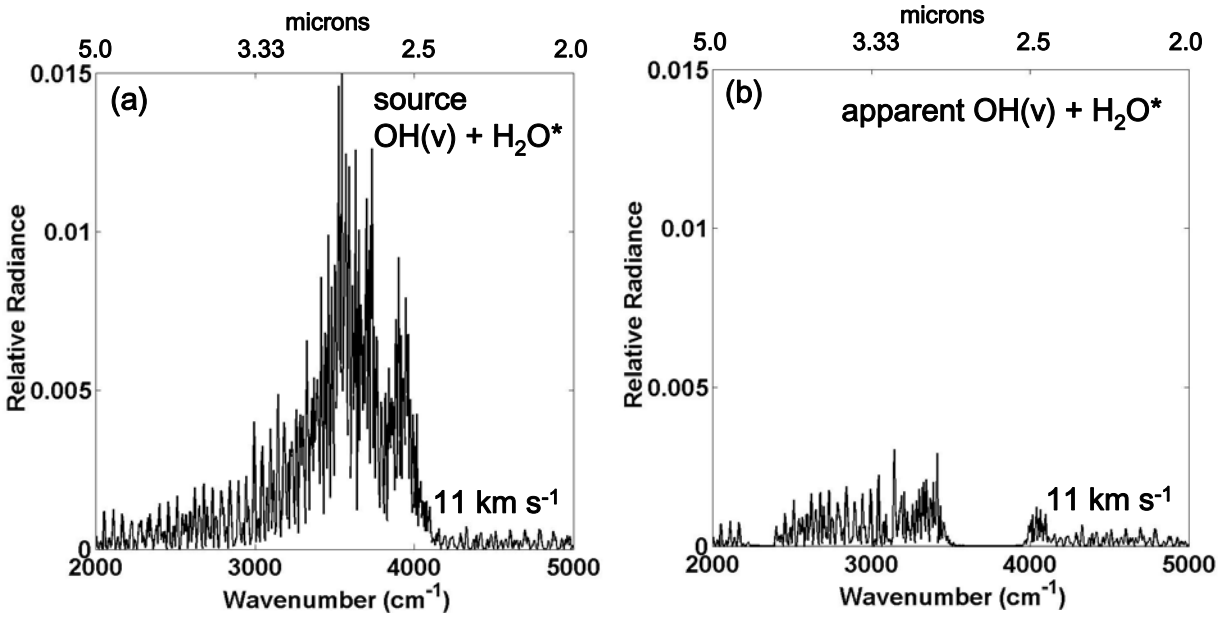

Fig. 9. (a) Source OH(v) + H_2O^* relative spectral radiance at 11 km s^{-1} relative collision velocity. (b) Apparent OH(v) + H_2O^* relative spectral radiance at 11 km s^{-1} relative collision velocity. Here the OH(v) + H_2O^* has been attenuated by the atmosphere.

It is useful to report the total signal in Watts integrated spatially over the entire radiating region and spectrally across 2-5 μm that would be observed from AMOS including atmospheric attenuation following the above analysis. We expect this estimate to be an upper bound on the observable radiation. We use the following equation, following Eq. 3, to perform the estimate,

Total Signal (Watts) = (Efficiency in photons per H_2O from Fig. 5) (# H_2O from engine s^{-1}) (3.33e3 cm^{-1} / photon) (1.9863e-23 Joules / cm^{-1}) (atmospheric attenuation factor) (5)

The results are given in the table below for 8 km s^{-1} and 11 km s^{-1}.

Table 1. Total signal estimates for shuttle PRCS engine firings including atmospheric attenuation in the 2-5 μm pass-band. Efficiencies include contributions from OH 2.8 μm, OH(v), and H_2O^*, H_2O 2.7 μm, as shown in Fig. 5.

Relative Velocity (km s^{-1})	Efficiency from Fig. 5 (OH 2.8 μm+ H_2O 2.7 μm)	PRCS Engine # H_2O s^{-1}	Atmospheric Attenuation	Total Signal (Watts)
8.0	0.0538	1.42e25	0.249	1.26e4
11.0	0.214	1.42e25	0.187	3.76e4

Previous observations from AMOS of two PRCS engine firings simultaneously at 11 km s^{-1} report a signal of 6.3e4 Watts ± 50% in a somewhat narrower spectral region [6,8]. For a single engine, as assumed in the present analysis, this gives an approximate total signal of 3.15e4 ± 50% Watts, which is well matched by the 3.76e4 Watts at 11 km s^{-1} given in Table 1.

6. INSTRUMENTATION

A total signal estimate from the space shuttle PRCS plume in the 2 – 5 μm band allows an assessment of available sensors and measurement feasibility. The basic measurement approach consists of integrating a spectrometer onto one of the large telescopes at the AMOS facility. The B37 1.2 m telescope has been identified as available for visiting experimenters [15]. This particular telescope has a 3 mrad total field-of-view (FOV) which would encompass only 2.3 km of plume assuming a 60^0 view angle from zenith. A telescope with at least 8 mrad FOV is really needed to collect most of the expected plume emission. The B37 telescope might still be acceptable since collecting a good spectrum is the priority, and as long as there is sufficient signal-to-noise (S/N). A good spectrum in this case would be a plume measurement at 4 cm^{-1} spectral resolution. This would allow identification of key reactions and species. Though a 4 cm^{-1} spectrum would be ideal, 8 or even 16 cm^{-1} would still be useful. Two different spectrometer systems are currently under consideration. These are discussed in the proceeding paragraphs along with some initial S/N estimates.

The small size, ruggedness, and fast scanning capability of ABB's (formerly Bomem) 200 series Fourier Transform Infrared (FTIR) Spectroradiometer make it a potential candidate. A currently available system operates with two simultaneous detectors; an InSb covering 1 – 6 μm and an MCT covering 2 – 15 μm. Its basic specifications are listed in Table 2 below. Both detectors are liquid nitrogen cooled. The 1 cm^{-1} Noise Equivalent Spectral Radiance (NESR) is 1.37e-09 and 1.4e-08 $W/cm^2\text{-}sr\text{-}cm^{-1}$ for the InSb and MCT detectors respectively. Both values were measured with a 1 sec integration time. The NESR at other resolutions and integrations times can be estimated from

$$NESR_\nu = \frac{NESR_1}{\nu\sqrt{t}} \tag{6}$$

where $NESR_1$ is the NESR at 1 cm^{-1}, ν is the wavenumber resolution, and t is the measurement time.

Table 2. ABB 254 FTIR Spectrometer Specifications

Resolution (cm^{-1})	1	2	4	8	16
Frame Rate (scans/sec)	10.3	18.6	31.4	47.8	64.6
Max Acquisition Time (sec)	95	104	125	163	242

Assuming the spectrometer FOV is filled (via some telescope system), a radiance can be generated using the total signal estimate from the preceding section and by assuming plume emission from a spherical region of space. An average apparent radiance is given by

$$L^a = \frac{P}{4\pi A} \tag{7}$$

where L^a is the apparent radiance, P is the total power in Watts, and A is the plume area. To calculate a S/N the NESR was converted to a Noise Equivalent Radiance (NER) by multiplying by the bandwidth (3000 cm^{-1}). This assumes a constant NESR over the 2 – 5 μm band which was found to be reasonable for this initial analysis. The S/N is then just given by

$$\frac{S}{N} = \frac{L^a}{NER}. \tag{8}$$

Figure 10 shows the calculated S/N for the InSb detector at the available spectral resolutions and up to 15 seconds of frame co-addition. A plume diameter of 5 km and a total signal of 3.76e04 W (11 km/s case) are assumed. The results are not encouraging as no S/N values were above 1. Further, the current configuration for the

B37 telescope would not meet the spectrometer total FOV assumption. The spectrometer collimator has a 45 mrad FOV and a 6.4 mm entrance aperture.

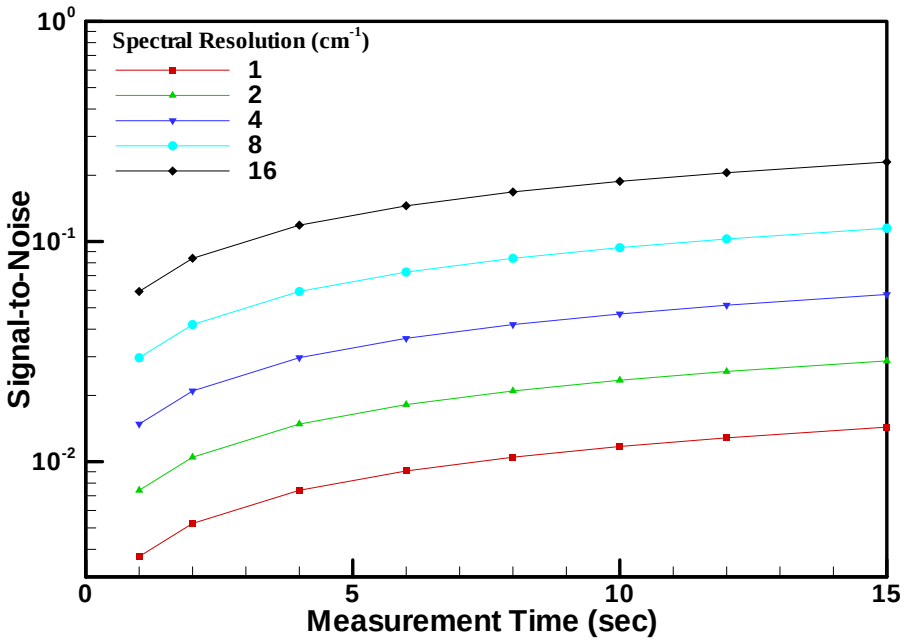

Figure 10. Estimated Signal-to-Noise for Various Spectrometer Spectral Resolutions and Measurement Times

The emission analysis did not include any H_2O or OH overtone radiation below 2 μm which could help improve the overall S/N. Also, the new 300 series spectrometer currently being offered by ABB has a factor of 2 improvement in sensitivity. But according the above results at least an order of magnitude and probably two orders of magnitude improved sensitivity are needed for a good measurement.

Another possible sensor is the Broadband Array Spectrograph System (BASS) owned and operated by the Aerospace Corporation [16]. It is a dispersive type spectrometer with a 3 -13.5 μm spectral range. This instrument has a stated noise equivalent power (NEP) of 4.0e-14 W/sqrt(Hz) for a 1 second integration time. The sensor would not capture any emission from OH or H_2O below 3 μm but most of that may be absorbed anyway (see Figure 9b). Since this instrument disperses the energy into separate detectors, a per-pixel S/N estimate was obtained. Unfortunately this required dividing the total signal estimate up into a spectrum. A rough estimate for the 3 – 4.2 μm (2400 – 3333 cm^{-1}) region was accomplished by assuming approximately 60% of the total energy was emitted equally over this region (see Figure 9b). Utilizing the radiance calculation from equation 7 and the solid angle of the AMOS B37 telescope a spectral irradiance was estimated with

$$E_\lambda = \frac{0.6 L^a \Omega_t}{\Delta\lambda}\ , \tag{9}$$

where Ω_t is the telescope solid angle and $\Delta\lambda$ is 1.2 μm. The S/N was then calculated from

$$\frac{S}{N} = \frac{E_\lambda A_t \Delta\lambda_d \sqrt{t}}{NEP}\ , \tag{10}$$

where A_t is the telescope primary mirror area, $\Delta\lambda_d$ is the approximate pixel spectral resolution (0.1 μm) in that wavelength region, and t is the detector integration time. Assuming a 1 sec integration time, a S/N of approximately 1448 was calculated. While this seems very encouraging, there would be a price. Near the 3 μm spectral region, a 0.1 μm difference between pixels translates to over 100 cm^{-1} difference in wavenumber. The spectral resolution would be far lower than that desired. As with the FTIR spectrometer, the analysis also assumed

that all the energy collected by the telescope was input into the BASS spectrometer. The results of these calculations for the BASS sensor were not reviewed and approved by any Aerospace Corp. personnel.

7. CONCLUSIONS AND FUTURE WORK

We have presented an estimate of the total signal level of radiation in the 2-5 μm region of Shuttle PRCS engine firings that could be observed from AMOS. The analysis is based on very recent work on the chemical mechanisms which give rise to the radiation, involving production of excited OH and H_2O species formed from collisions of atmospheric O-atom and H_2O from the engine exhaust. Our analysis includes effects of the attenuating atmosphere and an estimate of the spectral distribution of radiation. Our results for the total signal are in good agreement with a previous observation from AMOS of PRCS engine firings, giving us confidence in the overall analysis.

One weakness of the present analysis involves assumptions about how much collisionally excited H_2O radiates in the 2-5 μm band. Future work will involve obtaining better estimates of the excited H_2O contribution through use of quantum scattering techniques. It may also be possible to extract this information from simulations of the excited H_2O spectra obtained from classical trajectory calculations [17]. Another important consideration in assessing the feasibility of ground-based observations is the spatial distribution of radiation. Modeling of the spatial distribution will require use of a reacting flow code and an analysis similar to that done in [3].

The initial analysis indicates that the ABB FTIR spectroradiometer would not have the sensitivity to measure the space shuttle plume emission under full FOV conditions. Perhaps, a large telescope with a short focal length (i.e. fast optics) could be one way to increase the signal into the ABB spectrometer. The BASS sensor, on the other hand, may have the sensitivity required, but at the cost of lower spectral resolution. Further investigation into various infrared spectrometers and telescope arrangements is clearly needed.

8. ACKNOWLEDGEMENTS

M.B. and L. S. acknowledge support through a Small Business Innovative Research (SBIR) award from the Missile Defense Agency (MDA) Contract No. F04611-03-C-0015 and support from the DoD through contract F19628-00-C-0006.

9. REFERENCES

1. G. E. Caledonia, “Infrared Radiation Produced in Ambient/Spacecraft-Emitted Gas Interactions Under LEO Conditions”, AIAA paper 00-0104 (2000).

2. Lawrence S. Bernstein, Rainer A. Dressler, Yu-hui Chiu, John O. Wise, James A. Gardner, A. Lyle Broadfoot, Matthew Braunstein, Paul Sydney, and Edmond Murad, “Temporal Dependence of the Spectral Content of LEO Spacecraft Engine-Exhaust Atmospheric Interactions”, 2004 AMOS Conference, Maui, HI.

3. W. L. Dimpfl, G. C. Light, and L. S. Bernstein, J. Spacecraft and Rockets, **42**, 352 (2005).

4. D. K. Zhou, W. R. Pendleton, Jr. G. E. Bingham, D. C. Thompson, W. J. Raitt, and R. M Nadile, J. Geo. Res. **99**, 19,585 (1994).

5. R. E. Meyerott, G. R. Swenson, E. L. Schweitzer, and D. G. Koch, J. Geo. Res. **99**, 17,559 (1994).

6. L. S. Bernstein, J. B. Elgin, C. P. Pike, D. J. Knecht, E. E. Murad, T. F. Zehnpfennig, G. E. Galicia, and A. T. Stair, Jr., J. Geo. Res. **101**, 383 (1996).

7. D. P. Murtagh, E. J. Llewellyn, and P. J. Espy, Geo. Res. Lett, **24**, 85 (1997).

8. D. L. A. Rall, I. L. Kofsky, C. P. Pike, D. J. Knecht, and T. P. Zehnpfennig, Journal of Spacecraft and Rockets, **33**, 393 (1996).

9. L. Bernstein, Y. Chiu, J. A. Gardner, A. L. Broadfoot, M. Lester, M. Tsiouris, R. Dressler, and E. Murad, J. Phys. Chem. **107**, 10695 (2003).

10. M. Braunstein, R. Panfili, R. Shroll, and L. Bernstein, J. Chem. Phys. **122**, 184307 (2005).

11. G. Karabadzhak, Y. Plastinin, E. Szhenov, A. Afanasiev, and B. Khmelinin, “Preliminary Analysis of Exhaust Plume Radiation during Soyuz-TM Retro-firings”, 34th AIAA Thermophysics Conference and Exhibit, AIAA Paper 2000-2373, Denver, CO, 2000.

12. P.K. Acharya, A. Berk, G. P. Anderson, N. F. Larsen, S..-Chee Tsay, and K. H. Stamnes, “MODTRAN4: Multiple Scattering and Bi-directional Reflectance Distribution (BRDF) Upgrades to MODTRAN”, SPIE Proceedings, Optical Spectroscopic Techniques and Instrumentation and Space Research III, Volume 3756, July 1999.

13. L.S. Rothman et al, “The HITRAN molecular spectroscopic database: edition of 2000 including updates through 2001, J. of Quantitative Spectroscopy and Radiative Transfer **82**, pp. 5-44 (2003).

14. R. L. Sundberg, J. W. Duff, and L. S. Bernstein, “Nonequilbrium infrared emission model for the wake flow of re-entry vehicles”, J. of Spacecraft and Rockets, vol 30, pp. 731-741 (1993).

15. AMOS User’s Manual, Det 15, Air Force Research Laboratory, Kihei, Maui, Hawaii, Rev 12, April 2001.

16. Hackwell, J. A., D. W. Warren, M. Chatelain, Y. Dotan, P. Li, D. K. Lynch, D. Mabry, R. W. Russell, and R. Young, "A Low Resolution Array Spectrograph for the 2.9 - 13.5 μm Spectral Region", Proc. SPIE Conference 1235 on Instrumentation in Astronomy VII (1235), 171-180 (1990).

17. Noid D. W., M.L. Koszykowski and R. A. Marcus, " A spectral analysis method of obtaining molecular spectra from classical trajectories", J. Chem. Phys., **67**, 404 (1977)